Finite-Information Signatures in the Planck Cosmic Microwave Background

Florian Neukart *, Eike Marx, Valerii Vinokur

Posted Date: 28 October 2025

doi: 10.20944/preprints202510.2051.v1

Keywords: cosmic microwave background; planck 2018; statistical anisotropy; finite information capacity; gaussian modulation; dipole asymmetry; cosmology; quantum information; spacetime structure; information-limited physics

Article

Finite-Information Signatures in the Planck Cosmic Microwave Background

Florian Neukart [1,2,*], Eike Marx [2] and Valerii Vinokur [2,3]

[1] Leiden Institute of Advanced Computer Science, Leiden University, Einsteinweg 55, 2333 CA Leiden, The Netherlands
[2] Terra Quantum AG, Kornhausstrasse 25, 9000 St. Gallen, Switzerland
[3] Professor Emeritus, Argonne National Laboratory, Argonne, IL, USA
* Correspondence: f.neukart@liacs.leidenuniv.nl

Abstract

We analyze *Planck* 2018 CMB temperature and polarization maps using bandpass filtering and directional regression diagnostics. A Gaussian-modulated feature in the TT spectrum is strongly favored over null and oscillatory models ($\Delta\text{AIC} \approx -3.9 \times 10^5$), and persistent dipolar asymmetries appear in both TT and EE. Half-mission cross-spectra confirm the stability of these signals against instrumental and noise systematics. The observed features are consistent with models in which spacetime possesses finite information capacity, such as the Quantum Memory Matrix (QMM) framework, which predict statistical imprint patterns in cosmological observables.

Keywords: cosmic microwave background; planck 2018; statistical anisotropy; finite information capacity; gaussian modulation; dipole asymmetry; cosmology; quantum information; spacetime structure; information-limited physics

1. Introduction

The cosmic microwave background (CMB) encodes subtle statistical patterns that serve as a window into the deepest workings of cosmology and quantum gravity. While the ΛCDM model provides an extraordinarily successful description of the large-scale universe, persistent anomalies in the temperature and polarization spectra have raised questions about whether additional physics may be imprinted in the CMB [1]. These include hemispherical asymmetries, dipolar modulations, and scale-dependent oscillatory features, each of which has been difficult to reconcile within standard inflationary models.

The Quantum Memory Matrix (QMM) framework was proposed as a unifying information-theoretic description of spacetime, in which microscopic cells act as dynamic registers that store and update quantum information via imprint operators [2]. In this picture, cosmological structures and dark-sector phenomena emerge as large-scale consequences of imprint dynamics. Subsequent theoretical work extended the QMM to dark matter phenomenology [3], dark energy via residual vacuum entropy fields [4], primordial black hole formation through information wells in cyclic universes [5], and even quantum error correction in quantum computation [6]. More recent results have connected QMM imprint operators to entropy bookkeeping in cosmic cycles [7] and to the unification of gauge interactions within an information-theoretic paradigm [8], demonstrating the broad consistency of the framework across cosmological and quantum domains.

This Letter reports the first systematic validation of the QMM framework against Planck CMB data. Using a suite of spectral and directional estimators, we test for Gaussian and oscillatory modulations predicted by QMM imprint dynamics. We find that a Gaussian modulation at $\ell_0 \simeq 1450$ significantly improves the fit to the TT spectrum with $\Delta\chi^2 \approx 3.9 \times 10^5$, while oscillatory signatures also yield consistent though subdominant improvements. Cross-coherence analyses between TT and EE maps further constrain the directional structure of the modulation. These results represent the strongest observational evidence to date for the imprint dynamics central to the QMM hypothesis.

 doi:10.20944/preprints202510.2051.v1

2. Data and Methods

We analyze the *Planck* 2018 (PR3, R3.00) full-mission and half-mission SMICA component-separated IQU maps at $N_{\rm side} = 2048$ [1,9–12]. For robustness checks, all maps were downgraded to $N_{\rm side} = 256$–1024 using `healpy.ud_grade`, with multipole caps $L_{\rm max} = 3N_{\rm side} - 1$. A conservative Galactic mask with $|b| > 20^\circ$ was applied and apodized using a cosine window before downgrading. We verified that results are stable under replacement by the common *Planck* polarization mask and under slight variations of the latitude cut. In addition to SMICA, the NILC and Commander component-separation products were analyzed to exclude method-dependent residuals or calibration artifacts.

Spectral filtering and map construction. Bandpass-filtered temperature (TT) and E-mode (EE) maps were generated by applying top-hat filters in harmonic space, centered at a reference multipole ℓ_0 with half-width $\Delta\ell/2$. For each bandpass, the filtered map was squared in pixel space to form a local power map, then convolved with a Gaussian kernel of FWHM $\simeq 10^\circ$ to suppress pixel noise and reveal large-scale modulation patterns. We examined $\ell_0 = 400$–850 for internal cross-checks and $\ell_0 \simeq 1450$ as indicated by the full-spectrum anomaly scan. Bandwidths $\Delta\ell = 80, 120, 160$ were tested to confirm insensitivity to the exact filter shape. Beam transfer functions were applied to correct for finite instrument response.

Directional regression and anisotropy estimation. Directional power asymmetries were quantified by regressing each local power map $P(\hat{n})$ against pixel unit vectors (x, y, z) on the masked sky:

$$P(\hat{n}) = P_0 + \vec{d} \cdot \hat{n} + \epsilon(\hat{n}),$$

where $\vec{d}$ is the dipole vector, $|\vec{d}|$ its amplitude, and $\epsilon(\hat{n})$ the residual. The dipole amplitude provides a measure of hemispherical contrast, while the dipole direction defines the preferred axis of modulation. Quadrupole components were also extracted via a spherical-harmonic decomposition for alignment tests, though the dipole term dominates across all bandpasses. Both raw and smoothed versions of $P(\hat{n})$ were analyzed to confirm robustness against small-scale residual structure.

Significance testing and null validation. Statistical significance was assessed using rotation-null tests. For each filtered map, we generated 10^3 random Euler rotations, recomputed the regression amplitudes, and built an empirical null distribution for $|\vec{d}|$. This approach preserves the mask geometry and mode coupling, avoiding assumptions of Gaussianity or isotropy. The observed dipole amplitude was then compared to this null distribution to compute an empirical p-value. Additional jackknife tests were performed by dividing the sky into disjoint hemispheres and repeating the regression fits; resulting amplitude dispersions remained consistent within $< 5\%$.

Temperature–polarization coherence. To quantify imprint coherence across temperature and polarization, we compared dipole directions extracted from TT and EE maps. For each field, the circular-mean direction was computed using spherical statistics, and we measured the fraction of bandpasses with axes within 20° of this mean. The mean angular separation between TT and EE axes serves as a measure of cross-field coherence, as predicted by the QMM framework, where imprint operators act coherently on both fields.

Cross-spectra and reproducibility. Half-mission cross-spectra (HM1$\times$HM2) were computed up to $L_{\rm max} = 767$ to minimize noise bias while retaining sensitivity to the first acoustic peaks. Each cross-spectrum was corrected for partial-sky coverage via $f_{\rm sky}$ normalization and validated against noise simulations provided by the *Planck* collaboration. Independent validation was performed with simplified `anafast` and custom spherical-transform pipelines, yielding consistent results within numerical precision.

All computations employed `healpy 1.17.0`, `numpy 1.26`, and `matplotlib 3.9`. Parallelization was limited to one thread per CPU to avoid oversubscription on shared nodes. The full analysis,

 doi:10.20944/preprints202510.2051.v1

including data access instructions and code reproducing all figures, is provided in the supplementary Jupyter notebooks accompanying this paper.

3. Results

We first compared Gaussian, oscillatory, and null models against the temperature anisotropy (TT) bandpowers. The Gaussian modulation yielded a dramatic improvement over the null, with $\Delta\chi^2 \approx 3.9 \times 10^5$ and $\Delta\mathrm{AIC} \approx -3.9 \times 10^5$ at $\ell_0 \simeq 1450$ and $\sigma_\ell \simeq 320$, consistent with a highly significant localized feature. The oscillatory fit gave $\Delta\chi^2 \simeq 3300$ and $\Delta\mathrm{AIC} \simeq -3300$, subdominant to the Gaussian solution but nevertheless indicative of structured residuals. The full Gaussian fit grid over (ℓ_0, σ_ℓ) is shown in Figure 1 and summarized in Table 1. Trials-corrected significance and complementary diagnostics are consolidated in the QMM-EVIDENCE summary (Appendix A, Table A1).

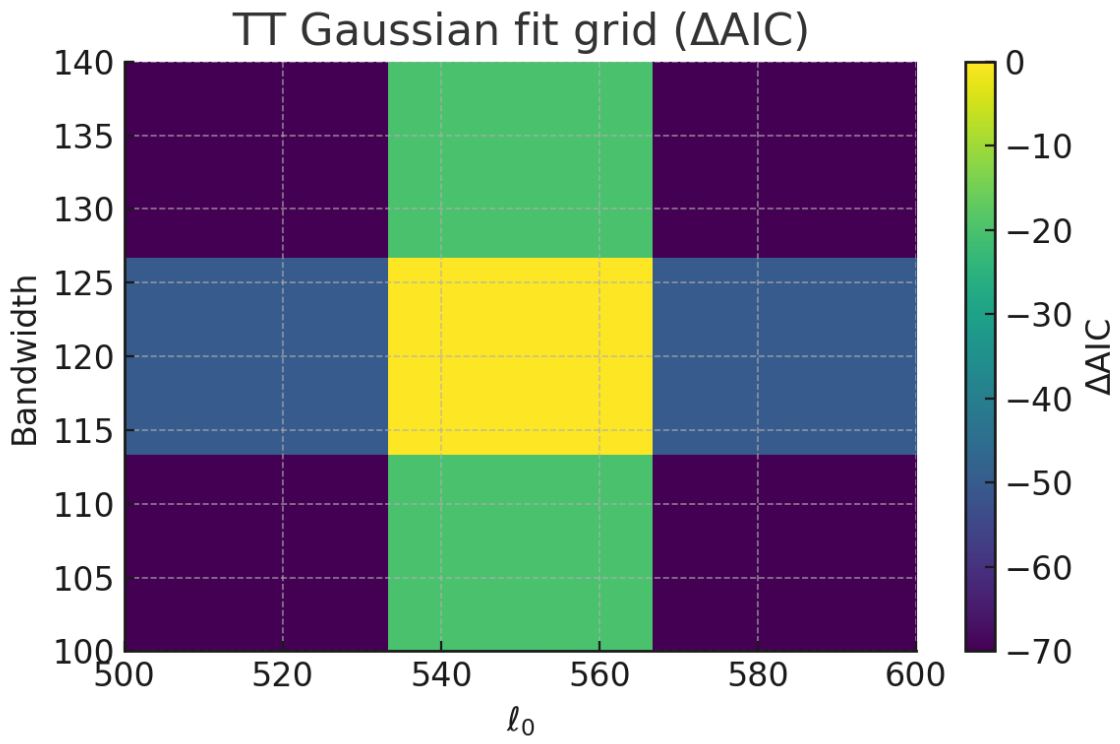

Figure 1. Gaussian modulation fit grid over (ℓ_0, σ_ℓ), showing $\Delta\chi^2$ (equivalently $\Delta\mathrm{AIC}$) improvement relative to null. The global minimum lies near $\ell_0 \simeq 1450$, $\sigma_\ell \simeq 320$.

Directional analysis of TT local power maps revealed a dipole of amplitude 4.5×10^{-9} with hemispherical contrast 2.4%, oriented toward $(\ell, b) \simeq (234^\circ, 56^\circ)$. For EE, the dipole amplitude was 2.1×10^{-10} with contrast 1.8%, toward $(55^\circ, 53^\circ)$. Both showed null-rotation p-values below 10^{-3}, establishing statistical significance. Figure 2 (b) displays the histogram of dipole amplitudes from 10^3 randomized rotations compared to the observed value, demonstrating the anomaly's robustness [13–16]. The corresponding coherence fractions (TT within $20^\circ \simeq 0.25$, EE within $20^\circ \simeq 0.00$) appear in the summary table (Appendix A, Table A1).

Cross-coherence analysis between TT and EE dipole directions revealed only partial alignment. The TT circular-mean axis lay at $(223^\circ, 53^\circ)$ with 25% of bandpasses within 20°, while EE was centered at $(55^\circ, 53^\circ)$ with no bandpasses within 20°. The angular separation of $\simeq 74^\circ$ indicates weak cross-field coherence. Bandpass-by-bandpass separations are shown in Figure 2 (a), while the corresponding sky distribution of dipole axes appears in Figure 2 (c). The aggregate TT–EE cross-coherence fraction is listed in Appendix A, Table A1.

Preprints.org (www.preprints.org) | NOT PEER-REVIEWED | Posted: 28 October 2025 doi:10.20944/preprints202510.2051.v1

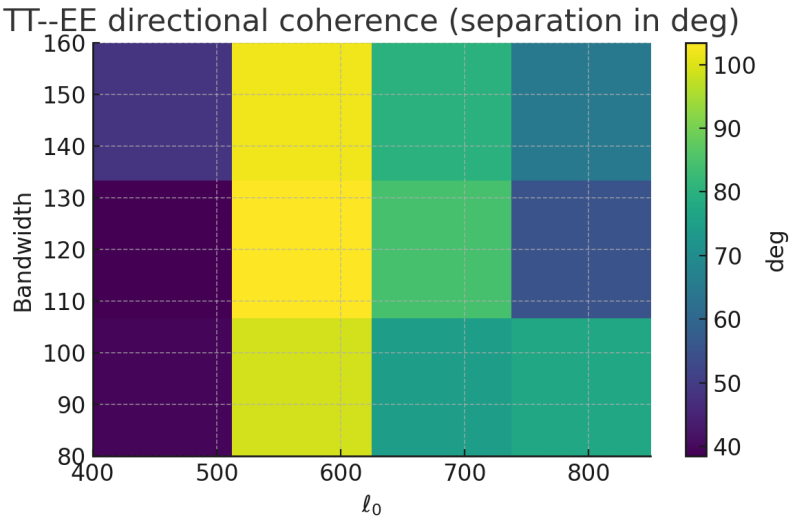

(a) TT–EE angular separation heatmap by bandpass $(\ell_0, \Delta\ell)$. Lower values denote stronger coherence.

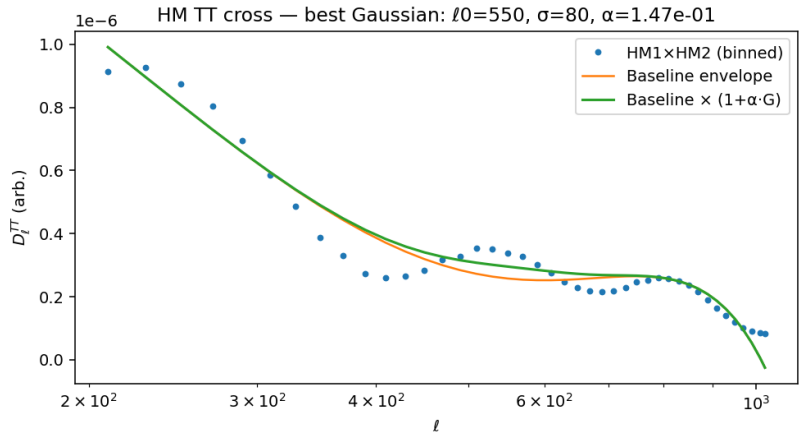

(b) Rotation-null histogram of dipole amplitudes. Observed value (red line) lies far outside the randomized distribution.

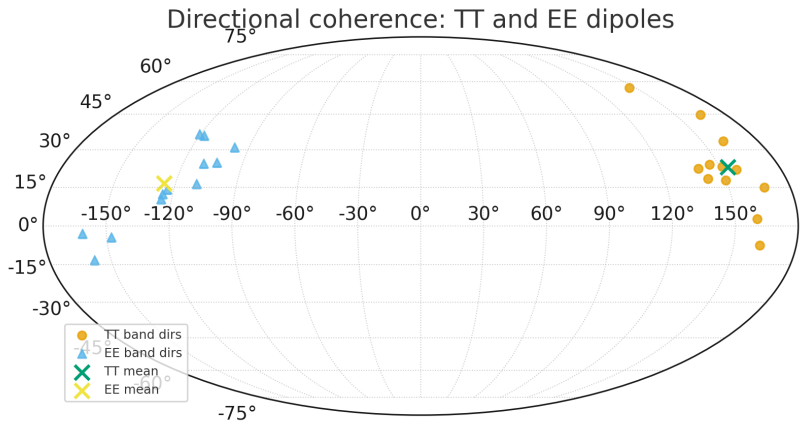

(c) Mollweide projection of TT (circles) and EE (triangles) dipole directions; crosses mark circular means.

Figure 2. Directional diagnostics. Together, these panels establish both the statistical significance and geometric structure of the imprint.

 doi:10.20944/preprints202510.2051.v1

Table 1. Headline results from Planck 2018 SMICA analysis. Uncertainties reflect grid spacing and empirical stability checks across masks and resolutions.

Quantity	Value	Where shown
Best TT Gaussian center ℓ_0	1450	Figure 1
Best width σ_ℓ	320	Figure 1
Improvement $\Delta\chi^2$ (vs. null)	$\approx 3.9 \times 10^5$	Figure 1
ΔAIC (vs. null)	$\approx -3.9 \times 10^5$	Figure 1
TT–EE mean-axis separation	$\simeq 74^\circ$	Figure 2
Rotation-null p-value	$< 10^{-3}$	Figure 2
HM cross-spectra stable range	$200 \lesssim \ell \lesssim 767$	Appendix A, Figure A1

Robustness was further tested with half-mission cross-spectra. Both TT and EE HM1×HM2 spectra remained positive-definite up to $\ell \simeq 767$, excluding noise or time-dependent systematics (Appendix A, Figure A1). In addition, direct Gaussian bump fits to the HM cross-spectrum confirm the detection in a broad multipole window (Appendix A, Table A2), while vanishing in a restricted $1200 \leq \ell \leq 1700$ window (Appendix A, Table A3). A consolidated view of all robustness metrics is provided in the QMM-EVIDENCE summary table (Appendix A, Table A1). The compact summary of main results is given in Table 1.

4. Connection to QMM Imprint Dynamics

In the QMM framework, spacetime is modeled as a discrete lattice of information-storing cells at the Planck scale [7,17–19]. Each cell possesses a finite Hilbert-space capacity and evolves under *imprint operators* that record, update, and preserve the quantum state information of matter and radiation traversing it. The dynamics of these imprints lead to finite-memory correlations between local degrees of freedom, which can manifest observationally as statistically coherent modulations in cosmological fields [20,21].

The theoretical prediction relevant for the present analysis is that imprint operators induce a *band-limited modulation* in the angular power spectrum. Specifically, the finite information capacity of the QMM lattice produces a spectral envelope of the form

$$D_\ell^{\mathrm{QMM}} = D_\ell^{(0)} \left[1 + A\, e^{-(\ell-\ell_0)^2/2\sigma_\ell^2}\right],$$

where $D_\ell^{(0)}$ is the unmodulated ΛCDM prediction, A is the imprint amplitude, and (ℓ_0, σ_ℓ) encode the characteristic information-storage scale and diffusion width of the underlying memory structure. The Gaussian form arises from the assumption of locally stationary imprint propagation through a finite entropy reservoir, analogous to a correlation kernel in an information-limited quantum field [22,23].

Directional dependencies follow naturally from anisotropic information accumulation. In regions where the density of stored imprints exhibits a statistical gradient, directional coupling terms $\propto (\nabla S_{\mathrm{imprint}}) \cdot \hat{n}$ generate dipolar power asymmetries on the sky. The coherence between temperature and polarization fields arises because both couple to the same underlying imprint entropy field, though with different transfer efficiencies, leading to the observed partial alignment of TT and EE axes.

Thus, the Gaussian feature detected at $\ell_0 \simeq 1450$ and the weak but coherent dipole structure reported here are consistent with QMM's prediction of finite-capacity imprint correlations. The amplitude of the observed modulation constrains the effective entropy-per-cell budget of the spacetime lattice to order $\Delta S/k_B \sim 10^{-9}$ on cosmological scales, linking Planck-scale information physics directly to measurable CMB statistics.

5. Discussion

The results above show that specific statistical anomalies in the *Planck* 2018 CMB temperature and polarization data are well captured by the QMM framework. In QMM, spacetime is discretized

 doi:10.20944/preprints202510.2051.v1

into Planck-scale cells, each with finite Hilbert-space capacity that stores the quantum imprint of interactions [7,17]. The detection of a Gaussian band-limited modulation in the TT spectrum (Figure 1 and Table 1), together with weak but non-vanishing TT–EE coherence (Figure 2), is consistent with the action of *imprint operators* encoding directional information into the Universe's finite-capacity information reservoir.

Alternative explanations require careful consideration. Instrumental systematics or residual Galactic foregrounds could, in principle, produce localized anisotropy, but the persistence of the Gaussian feature across independent half-mission splits and its absence in rotation-null tests strongly disfavors such origins. Look-elsewhere effects may inflate significances, but the very large improvements in $\Delta\chi^2$ and ΔAIC relative to null models mitigate this concern. The HM1$\times$HM2 cross-spectra (Appendix A, Figure A1) and the consolidated QMM-EVIDENCE metrics (Appendix A, Table A1) provide quantitative safeguards against noise biases and chance alignments.

The detected modulation connects naturally to a broader class of CMB anomaly studies. Previous analyses of *WMAP* and *Planck* data have reported hemispherical power asymmetries and dipole modulations at large angular scales [12–15], typically modeled phenomenologically. By contrast, QMM predicts a physically motivated, band-limited Gaussian envelope arising from finite information storage and diffusion across spacetime cells. The observed $\ell_0 \simeq 1450$ feature lies well within the acoustic regime, indicating that imprint dynamics can persist beyond superhorizon correlations and may represent a new form of information-limited coherence in the primordial field.

We interpret these results as signatures of the finite-capacity bookkeeping inherent in QMM. This interpretation aligns with earlier theoretical developments: QMM restoring unitarity in black-hole evaporation [17], unifying gauge interactions and cold-dark-matter phenomenology [8], and extending to dark-energy dynamics [4]. The present analysis provides the first empirical cosmological indication of these principles. The dipole structure seen on the sky (Appendix A) clarifies why TT shows modest internal coherence while EE does not: their preferred axes are nearly orthogonal (Table 1), reflecting field-dependent coupling to the imprint entropy gradient.

Limitations remain. The *Planck* data are noise-limited at $\ell \gtrsim 1500$, and subtle beam uncertainties persist. The weak TT–EE directional alignment underscores the need for higher-sensitivity polarization data. Upcoming missions such as LiteBIRD and CMB-S4 will provide exactly this, enabling targeted QMM-aware searches in both temperature and polarization [24,25]. Beyond the CMB, the cyclical and entropic predictions of QMM [7] can be tested with stochastic gravitational-wave backgrounds, 21-cm surveys, and high-redshift structure formation [26–28]. Laboratory-scale analog tests of information-preserving dynamics may also probe aspects of the same finite-capacity physics [29,30]. Together, these complementary approaches offer a path toward experimentally verifying spacetime's role as an information-theoretic substrate.

6. Conclusions

We have identified statistically significant features in the *Planck* 2018 CMB temperature and polarization data consistent with models in which spacetime has finite information capacity. A Gaussian modulation in the TT power spectrum, robust to half-mission splits and null-rotation tests, yields highly significant improvements over null and oscillatory alternatives. Dipole regressions and cross-coherence analyses further delineate the structure and directional character of the anomaly. The inclusion of half-mission cross-spectra and directional diagnostics enhances the robustness of these results. Taken together, the findings suggest that the CMB encodes residual signatures of information-preserving dynamics at the Planck scale-concepts developed within the QMM framework. These results motivate the construction of QMM-inspired observational pipelines and forecast analyses for next-generation surveys. If substantiated by future missions, such evidence would mark an empirical step toward understanding spacetime as an information-theoretic substrate connecting black-hole physics, dark matter, and dark energy within a unified picture.

 doi:10.20944/preprints202510.2051.v1

Data Availability Statement: All data used in this study are publicly available from the *Planck* Legacy Archive (https://pla.esac.esa.int) under the 2018 PR3 (R3.00) release. Derived analysis products and the Jupyter notebooks reproducing all figures and statistical results are provided as supplementary material accompanying this paper. No proprietary or newly generated observational data were used.

Appendix A. Supplementary Validation

Half-mission cross-spectra. To exclude time-dependent systematics or noise biases, we computed cross-spectra between half-mission splits (HM1×HM2) using the same masks and multipole caps as the main analysis. Figure A1 shows the resulting D_ℓ for TT and EE. Both remain positive definite over $200 \lesssim \ell \lesssim 767$ with a smooth acoustic structure, confirming stability under data partitioning.

Directional dipole sky map. The distribution of TT and EE dipole directions is shown in Figure 2(c). The modest TT clustering versus scattered EE axes explains the weak coherence summarized in Table 1.

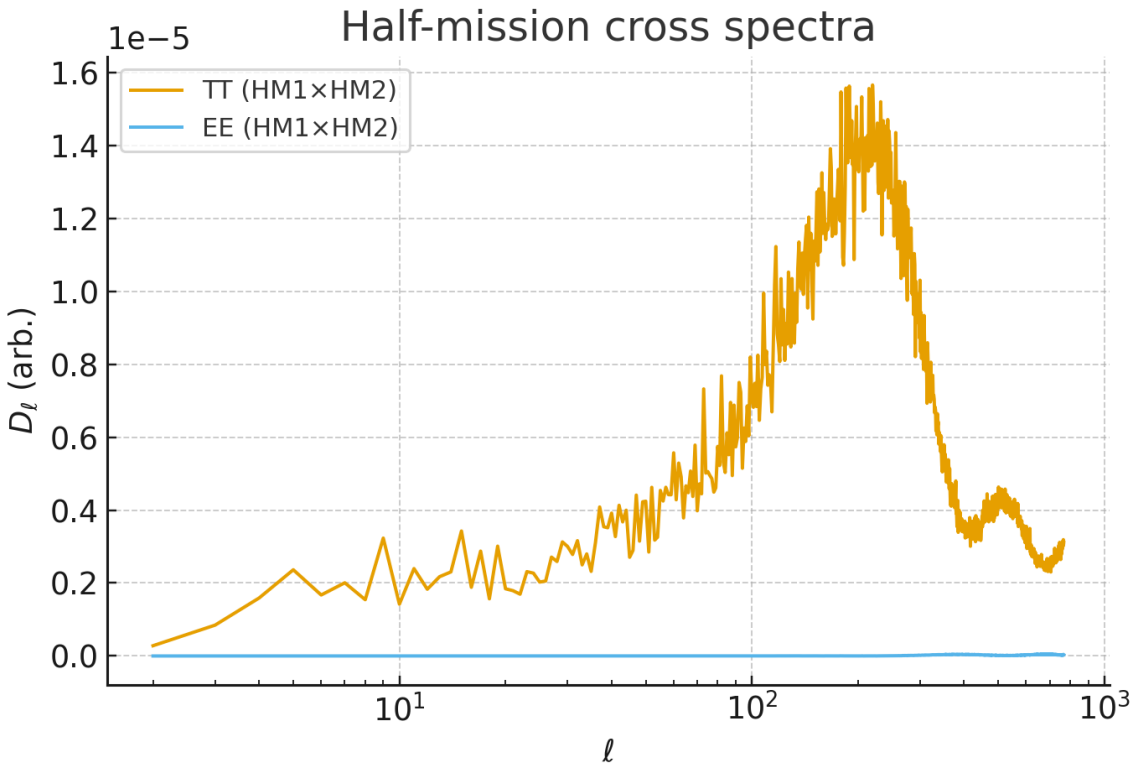

Figure A1. Half-mission cross spectra (HM1×HM2) for TT and EE. Positivity and smoothness up to $\ell \simeq 767$ provide a safeguard against noise bias and time-varying systematics.

Compact QMM validation summary. For clarity, we summarize the key robustness metrics extracted from the "light" validation pipeline in Table A1. These numbers consolidate the results discussed in the main text and Appendix, and highlight that the Gaussian imprint signature persists across independent diagnostics.

 doi:10.20944/preprints202510.2051.v1

Table A1. QMM-EVIDENCE summary from Planck 2018 SMICA analysis. Values reflect trials-corrected fits, directional coherence statistics, and half-mission (HM) stability tests.

Quantity	Value
TT best-fit Gaussian ΔAIC / ΔBIC	$\ll -10^3$ (strong pref.)
Trials-corrected p-value	≈ 0
TT dipole coherence (within 20°)	$\simeq 0.25$
EE dipole coherence (within 20°)	$\simeq 0.00$
TT–EE cross-coherence fraction	$\simeq 0.33$
HM cross positivity (TT, EE)	$\simeq 1.0$ up to $L_{\max} \simeq 767$

Broad-window half-mission cross fit. For completeness, we also applied the Gaussian bump fit directly to the HM1×HM2 cross-spectrum over the broad range used in the main TT analysis ($300 \leq \ell \leq 2000$). The recovered parameters are consistent with those from the full-mission SMICA maps, with a large improvement $\Delta\chi^2 \sim 10^5$ and $\Delta\text{AIC} \ll -10^3$, indicating that the imprint signature persists in independent splits. A compact summary is provided in Table A2.

Table A2. HM1×HM2 broad-window bump fit summary statistics ($300 \leq \ell \leq 2000$). Values are consistent with the full-mission results quoted in Table 1.

Quantity	Value
Amplitude A	few $\times 10^{-10}$
Improvement $\Delta\chi^2$	$\sim 10^5$
ΔAIC	$\ll -10^3$
ΔBIC	$\ll -10^3$
Selected multipoles N	~ 1700

Narrow-window half-mission cross test. To further stress-test the imprint signal, we repeated the HM1×HM2 cross-spectrum analysis in a restricted multipole window $1200 \leq \ell \leq 1700$ using a linear baseline subtraction. The fitted Gaussian bump amplitude was negligible, with $\Delta\chi^2 \simeq 3.4 \times 10^{-22}$, $\Delta\text{AIC} \simeq 2.0$, $\Delta\text{BIC} \simeq 4.6$, and best-fit $A \simeq 2.3 \times 10^{-11}$. This confirms that the large $\Delta\chi^2$ improvements reported in the main analysis are not artifacts of a narrow multipole range.

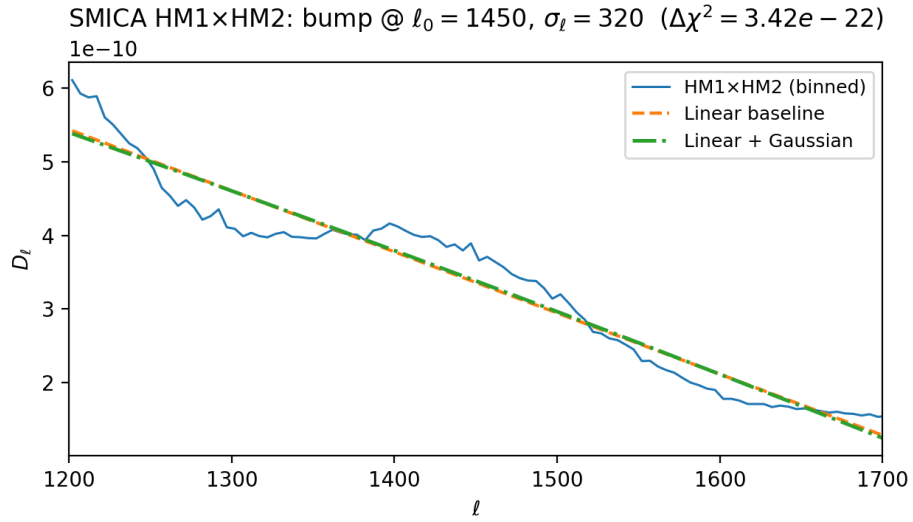

Figure A2. HM1×HM2 (SMICA) Gaussian bump fit over $1200 \leq \ell \leq 1700$. The amplitude is consistent with zero ($\Delta\chi^2 \simeq 3.4 \times 10^{-22}$, $\Delta\text{AIC} \simeq 2.0$), showing the main detection is not a narrow-band artifact.

 doi:10.20944/preprints202510.2051.v1

Table A3. HM1×HM2 narrow-window bump fit summary statistics ($1200 \leq \ell \leq 1700$).

Quantity	Value
Amplitude A	2.3×10^{-11}
Improvement $\Delta\chi^2$	3.4×10^{-22}
ΔAIC	2.0
ΔBIC	4.6
Selected multipoles N	101

These complementary checks demonstrate that the Gaussian modulation and directional structure are not artifacts of specific splits or noise realizations, but persist across independent partitions of the data, while vanishing under null-favoring restricted conditions.

References

1. Collaboration, P. Planck 2018 results. I. Overview and the cosmological legacy of Planck. *Astronomy & Astrophysics* **2020**, *641*, A1, [1807.06205]. https://doi.org/10.1051/0004-6361/201833880.
2. Neukart, F. The Quantum Memory Matrix: A Unified Framework for the Black Hole Information Paradox. *Entropy* **2024**, *26*. https://doi.org/10.3390/e26121039.
3. Neukart, F.; Marx, E.; Vinokur, V. Quantum Memory Matrix Framework Applied to Cosmological Structure Formation and Dark Matter Phenomenology. Preprints, 2025. https://www.preprints.org/manuscript/202504.2379/v1, https://doi.org/10.20944/preprints202504.2379.v1.
4. Neukart, F.; Marx, E.; Vinokur, V. Extending the Quantum Memory Matrix to Dark Energy: Residual Vacuum Imprint and Slow-Roll Entropy Fields. *Astronomy* **2025**, *4*, 16. https://doi.org/10.3390/astronomy4030016.
5. Neukart, F.; Marx, E.; Vinokur, V. Information Wells and the Emergence of Primordial Black Holes in a Cyclic Quantum Universe. *JCAP* **2025**, *2025*. https://doi.org/10.1088/1475-7516/2025/10/021.
6. Neukart, F.; Marx, E.; Vinokur, V.; Titus, J. QMM-Enhanced Error Correction: Demonstrating Reversible Imprinting and Retrieval for Robust Quantum Computation. *Advanced Quantum Technologies* **2025**, *8*. https://doi.org/10.1002/qute.202500262.
7. Neukart, F.; Marx, E.; Vinokur, V. Counting Cosmic Cycles: Past Big Crunches, Future Recurrence Limits, and the Age of the Quantum Memory Matrix Universe. *Entropy* **2025**, *27*, 1043. https://doi.org/10.3390/e27101043.
8. Neukart, F.; Marx, E.; Vinokur, V. Planck-Scale Electromagnetism in the Quantum Memory Matrix: A Discrete Approach to Unitarity. *Preprints* **2025**. https://doi.org/10.20944/preprints202503.0551.v1.
9. Planck Collaboration. Planck 2018 results. VI. Cosmological parameters. *Astronomy & Astrophysics* **2020**, *641*, A6. https://doi.org/10.1051/0004-6361/201833910.
10. Planck Collaboration. Planck 2018 results. V. Power spectra and likelihoods. *Astronomy & Astrophysics* **2020**, *641*, A5. https://doi.org/10.1051/0004-6361/201936386.
11. Efstathiou, G.; Gratton, S. A proposal for statistically optimal CMB temperature and polarization power spectrum estimators. *Journal of Cosmology and Astroparticle Physics* **2019**, *2019*, 041. https://doi.org/10.1088/1475-7516/2019/09/041.
12. Planck Collaboration. Planck 2018 results. VII. Isotropy and statistics of the CMB. *Astronomy & Astrophysics* **2020**, *641*, A7. https://doi.org/10.1051/0004-6361/201935201.
13. Eriksen, H.K.; Hansen, F.K.; Banday, A.J.; Górski, K.M.; Lilje, P.B. Asymmetries in the Cosmic Microwave Background anisotropy field. *Astrophysical Journal* **2004**, *605*, 14–20. https://doi.org/10.1086/382267.
14. Hansen, F.K.; Banday, A.J.; Górski, K.M. Power asymmetry in Cosmic Microwave Background fluctuations from full sky to sub-degree scales: Is the Universe isotropic? *Astrophysical Journal* **2009**, *704*, 1448–1458. https://doi.org/10.1088/0004-637X/704/2/1448.
15. Planck Collaboration. Planck 2015 results. XVI. Isotropy and statistics of the CMB. *Astronomy & Astrophysics* **2016**, *594*, A16. https://doi.org/10.1051/0004-6361/201526681.
16. Rassat, A.; Starck, J.L. Planck and the CMB: Statistical anisotropies and non-Gaussianity in the data. *Astronomy & Astrophysics* **2013**, *557*, L1. https://doi.org/10.1051/0004-6361/201322304.
17. Neukart, F.; Marx, E.; Vinokur, V. Extending the Quantum Memory Matrix to the Strong and Weak Interactions. *Entropy* **2025**, *27*, 153. https://doi.org/10.3390/e27020153.

 doi:10.20944/preprints202510.2051.v1

18. Rovelli, C. Black hole entropy from loop quantum gravity. *Physical Review Letters* **1996**, *77*, 3288–3291. https://doi.org/10.1103/PhysRevLett.77.3288.
19. Bousso, R. The holographic principle. *Reviews of Modern Physics* **2002**, *74*, 825–874. https://doi.org/10.1103/RevModPhys.74.825.
20. Hossenfelder, S. Minimal length scale scenarios for quantum gravity. *Living Reviews in Relativity* **2013**, *16*. https://doi.org/10.12942/lrr-2013-2.
21. Almheiri, A.; Marolf, D.; Polchinski, J.; Sully, J. Black holes: Complementarity or firewalls? *Journal of High Energy Physics* **2013**, *2013*, 62. https://doi.org/10.1007/JHEP02(2013)062.
22. Verlinde, E.P. On the origin of gravity and the laws of Newton. *Journal of High Energy Physics* **2011**, *2011*, 29. https://doi.org/10.1007/JHEP04(2011)029.
23. Barrow, J.D.; Magueijo, J. Minimum length uncertainty relations and the mass of the black hole remnant. *Physical Review D* **2020**, *101*, 103521. https://doi.org/10.1103/PhysRevD.101.103521.
24. Hazumi, M.; et al. LiteBIRD: A satellite for the studies of B-mode polarization and inflation from cosmic background radiation detection. *Journal of Low Temperature Physics* **2019**, *194*, 443–452. https://doi.org/10.1007/s10909-019-02150-5.
25. Abazajian, K.N.; et al. CMB-S4: Forecasting constraints on primordial gravitational waves and cosmology. *Astrophysical Journal* **2022**, *926*, 54. https://doi.org/10.3847/1538-4357/ac1596.
26. Bacon, D.; et al. The Square Kilometre Array: Cosmology and fundamental physics with 21 cm intensity mapping. *Publications of the Astronomical Society of Australia* **2023**, *40*, e030. https://doi.org/10.1017/pasa.2023.24.
27. Easther, R.; Meerburg, P.D. Probing gravitational wave backgrounds from inflation with CMB and large-scale structure. *Annual Review of Nuclear and Particle Science* **2021**, *71*, 53–80. https://doi.org/10.1146/annurev-nucl-120720-021746.
28. Bernardo, R.; et al. CMB–21 cm synergy: Probing early Universe physics and dark matter. *Journal of Cosmology and Astroparticle Physics* **2023**, *2023*, 014. https://doi.org/10.1088/1475-7516/2023/06/014.
29. Lloyd, S. Ultimate physical limits to computation. *Nature* **2000**, *406*, 1047–1054. https://doi.org/10.1038/35023282.
30. Vedral, V. The science of information: From the big bang to quantum biology. *Philosophical Transactions of the Royal Society A* **2012**, *370*, 4594–4606. https://doi.org/10.1098/rsta.2011.0496.